Finite size effects on kaonic pasta structures

Toshiki Maruyama,[1,*] Toshitaka Tatsumi,[2,†] Dmitri N. Voskresensky,[3,4,‡]
Tomonori Tanigawa,[5,1] Tomoki Endo,[2,§] and Satoshi Chiba[1,¶]

[1] *Advanced Science Research Center, Japan Atomic Energy Research Institute**, Tokai, Ibaraki 319-1195, Japan*
[2] *Department of Physics, Kyoto University, Kyoto, 606-8502, Japan*
[3] *Moscow Institute for Physics and Engineering, Kashirskoe sh. 31, Moscow 115409, Russia*
[4] *Gesellschaft für Schwerionenforschung mbH, Planckstr. 1, 64291 Darmstadt, Germany*
[5] *Japan Society for the Promotion of Science, Tokyo 102-8471, Japan*

(Dated: February 9, 2008)

Non-uniform structures of mixed phases at the first-order phase transition to charged kaon condensation are studied using a density functional theory within the relativistic mean field model. Including electric field effects and applying the Gibbs conditions in a proper way, we numerically determine density profiles of nucleons, electrons and condensed kaons. Importance of charge screening effects is elucidated and thereby we show that the Maxwell construction is effectively justified. Surface effect is also studied to figure out its effect on the density profiles.

I. INTRODUCTION

Concerning phase transitions in nuclear matter, various scenarios have been discussed, like e.g. liquid-gas transition [1], pion condensation [2], hadron-quark deconfinement transition [3, 4, 5, 6, 7, 8, 9], transitions between different color superconducting phases [10, 11, 12, 13], quark ferromagnetic transition [14], charged ρ meson condensation [15, 16], etc., and kaon condensation. In most cases these are first-order phase transitions (FOPTs).

References [17, 18, 19, 20, 21, 22, 23, 24, 25, 26, 27] and many others studied possibilities of s-wave kaon condensations, whereas Refs. [28, 29] considered also those of p-wave condensations. It has been argued (see [17, 18, 19, 20, 21, 22, 23, 24, 25, 26, 27, 28, 29] and references therein) that the FOPT to a K^- condensate state might occur in neutron stars already at densities only several times larger than the nuclear saturation density ρ_0.

The possibility of the FOPT to the kaon condensate state may lead to interesting consequences for physics of neutron stars, such as a delayed collapse of a supernova to a low-mass black hole, a fast cooling mechanism of neutron stars due to the opening up of the nucleon direct Urca process under a background of the charged kaon condensate, etc [20, 30, 31, 32, 33, 34, 35, 36].

Reference [3] argued that in systems with different charged species the structured mixed phases might appear due to the FOPT. For example in case of the nuclear matter below the saturation density, where the liquid-gas FOPT is relevant, the "nuclear pasta" structures have been studied by many authors [8, 37, 38, 39, 40, 41, 42, 43, 44, 45, 46, 47, 48, 49].

The physical reason for the possibility of the mixed (pasta) phases with different geometrical structures is that the charge neutrality may hold only globally rather than locally as in the Maxwell construction. Mechanically, a balance between the Coulomb force and the surface tension is responsible for the occurrence of the spatially non-uniform structures.

The appearance of the pasta structures could have important consequences for the various neutron star phenomena. If appeared at an early stage of the neutron star evolution the pasta could cause a drastic change of the neutrino opacity. It may influence the subsequent neutron star cooling, it affects the matter resistance to the stress and consequently the glitch phenomena, etc.

Long time there existed a naive view that not all the Gibbs conditions can be satisfied in a description by the Maxwell construction [3, 23, 24, 25], because the local charge neutrality is implicitly assumed in it. As the result of previous works, cf. [23, 24, 25], it was suggested that a broad region of kaonic pasta as a mixed phase may occur in neutron stars with various geometrical structures of the kaon condensed phase (dense phase) embedded in usual nuclear matter phase (dilute phase). However, in recent papers [6, 7, 8, 9, 50, 51] we have demonstrated that both treatments using the Gibbs conditions and the Maxwell construction are actually in agreement with each other, if one properly includes electric field effects. The bare Coulomb field is screened by rearranged charged particles. Taking first the hadron-quark phase transition as an explicit example [6, 7, 9], we showed that with screening effects included the most realistic parameter choice (density, chemical potentials, surface tension, etc.) does not allow the mixed phase due to the mechanical instability of structures. Thus if exists, the density region of the structured mixed phase should be largely limited.

In subsequent papers [8, 48, 49], we have explored the charge screening effect on the nuclear pasta phases at sub-nuclear densities. We compared the full calculation

**Present name: Japan Atomic Energy Agency
*Electronic address: maruyama.toshiki@jaea.go.jp
†Electronic address: tatsumi@ruby.scphys.kyoto-u.ac.jp
‡Electronic address: D.Voskresensky@gsi.de
§Electronic address: endo@ruby.scphys.kyoto-u.ac.jp
¶Electronic address: chiba.satoshi@jaea.go.jp

with those either not including the screening at all or including it only non-systematically, as has been performed in previous works. We found that the screening effect, being systematically treated, significantly affects the density range of the nuclear pasta with various geometries, while it results in only minor corrections to the EOS. We have also emphasized that the proton spatial rearrangement effect resulting in a screening is much more efficient, compared with the electron screening, because the proton Debye screening length is essentially smaller than the electron one. However, since the charge density as well as the baryon number density are rather low in the nuclear pasta case, the screening effect is still not so prominent compared to that we find for denser systems.

In this paper we continue our research [6, 7, 8, 9, 48, 49] of the special role of the charge screening effects in the problem of the construction of the mixed phases, taking s-wave kaon condensation as a further example, cf. brief notes [50, 51]. We study whether the kaonic pasta appears in dense neutron star matter, and examine the validity of the Maxwell construction for the practical use.

One may believe that models taking into account the chiral symmetry are more realistic for the treatment of the kaon condensation. Actually many works have been done using this approach [17, 18, 19, 20, 27]. However, we will exploit here a non-chiral model since the bulk calculations performed within chiral models do not allow the mixed phase [21, 27, 52]. Previous investigations of the kaon mixed phase [21, 22, 23, 24, 25, 26] were performed in a framework of the RMF models. Therefore we will also exploit a RMF model for a more straight comparison with the previously obtained results.

We also will figure out the surface effect. There are few works about this matter so far [25, 26, 53], and the finite size effects of the Coulomb interaction and the surface tension are still not elucidated. In Ref. [25] authors discussed the surface effect and derived the surface tension between the normal nuclear matter phase and the kaon condensed phase by considering two semi-infinite matters omitting the Coulomb interaction. They suggested that the kinetic terms consisting of space gradients of the σ, ω, ρ mean-fields affect only slightly the density profiles and the resulting surface tension. Therefore they omitted these kinetic terms while they kept the kinetic term of the kaon field. This scale of the kaon field then determines the change of all meson fields and the nucleon fields, as well as the resulting surface tension, see their Fig. 1. Then, they find the surface tension which is now determined by this single length-scale. After that, for different geometries minimizing the surface plus the Coulomb energy per volume in the structure size one may find the optimum structure size and the geometry. Note that the Coulomb energy density in their approach is given by the bare Coulomb potential decoupling with other fields. In reality this approximation does not hold. The scale of the change of the kaon field proves to be of the same order of magnitude as the scale of the change of the electric field, i.e. the Debye screening length. A variation of the electric field significantly affects the kaon distribution and vise versa. Therefore, we must discuss the surface effect by the kaon field and other meson mean-fields, separately: only short-scale fields can decouple with long-scale fields and thus the contribution of the former fields may be replaced by the phenomenological surface-tension parameter, whereas long-scale fields should be treated explicitly.

In Ref. [26] the authors omitted kinetic terms of the mean σ, ω, ρ fields (neglecting also the corresponding surface tension effect) and discussed the charge screening effect. By numerical analysis they demonstrated how much the screening effect may affect the density profiles for the kaon droplet phase.

We consistently incorporate the Coulomb field as the gauge field coupled with other fields of charged particles and we keep kinetic terms of all mean fields. We demonstrate that the σ, ω, ρ fields are the short-scale fields. Thus we treat consistently the long-range effects, such as screening, and the short-range effects and we show their interplay for the kaonic pasta. This we believe gives a new insight into the finite size effects in the mixed phase. Also by artificial variation of the scale of the short-range fields we demonstrate effects that can be reduced to the surface tension.

The paper is organized as follows. In Sect. II we introduce the thermodynamic potential and equations of motion for fields. In Sect. III we numerically solve the Poisson equation and the mean field equations to find the electric potential profile and the density profiles. We also derive the EOS and the phase diagram for the kaonic pasta. In Sect. IV we discuss the screening effect and the surface effect on the kaonic pasta. Our conclusions are drown in Sect. V. Details of the perturbative treatment of the Coulomb effect, which we refer to as the "no Coulomb" approximation, are deferred to Appendix A.

II. THERMODYNAMIC POTENTIAL AND NUMERICAL PROCEDURE

A. Thermodynamic potential

Let us present our framework to study kaonic pasta structures. Following the idea of the density functional theory within the RMF model, we can formulate equations of motion to study non-uniform nuclear matter numerically, cf. [54]. The RMF model with fields of mesons and baryons introduced in a Lorentz-invariant way is relatively simple for numerical calculations, but on the other hand it is sufficiently realistic to reproduce bulk properties of finite nuclei as well as the saturation properties of nuclear matter [49]. In our framework, the Coulomb interaction is properly included in equations of motion for nucleons and electrons and for meson mean fields, and we solve the Poisson equation for the Coulomb potential $V_{\rm Coul}$ self-consistently with those equations. Thus the baryon and electron density profiles, as well as the meson mean fields, are determined in a way fully consistent

with the Coulomb interaction.

We start with the thermodynamic potential for the system of neutrons, protons, electrons and mesons including kaons

$$\Omega = \Omega_N + \Omega_M + \Omega_e + \Omega_K. \quad (1)$$

The first term

$$\Omega_N = \sum_{a=p,n} \int d^3r \left[\int_0^{k_{\mathrm{F},a}} \frac{d^3k}{4\pi^3} \sqrt{{m_N^*}^2 + k^2} - \rho_a \nu_a \right] \quad (2)$$

is the contribution of nucleons with the local Fermi momenta $k_{\mathrm{F},a}(\mathbf{r}); a = n, p$, $m_N^*(\mathbf{r}) = m_N - g_{\sigma N}\sigma(\mathbf{r})$ is the effective nucleon mass and m_N is the nucleon mass in the vacuum. Nucleons couple with σ, ω and ρ mesons and thereby,

$$\begin{aligned} \nu_n(\mathbf{r}) &= \mu_n - g_{\omega N}\omega_0(\mathbf{r}) + g_{\rho N} R_0(\mathbf{r}), \quad (3) \\ \nu_p(\mathbf{r}) &= \mu_p + V_{\mathrm{Coul}}(\mathbf{r}) - g_{\omega N}\omega_0(\mathbf{r}) - g_{\rho N} R_0(\mathbf{r}), \end{aligned}$$

where μ_n and μ_p are neutron and proton chemical potentials and $g_{\sigma N}$, $g_{\omega N}$ and $g_{\rho N}$ are coupling constants between corresponding fields.

The second term in (1) incorporates the scalar (σ) and vector (ω_0, R_0) mean fields,

$$\begin{aligned} \Omega_M &= \int d^3r \left[\frac{(\nabla\sigma)^2 + m_\sigma^2\sigma^2}{2} + U(\sigma) \right. \\ &\left. - \frac{(\nabla\omega_0)^2 + m_\omega^2\omega_0^2}{2} - \frac{(\nabla R_0)^2 + m_\rho^2 R_0^2}{2} \right], \quad (4) \end{aligned}$$

where m_σ, m_ω and m_ρ are the field masses, and $U(\sigma) = \frac{1}{3}bm_N(g_{\sigma N}\sigma)^3 + \frac{1}{4}c(g_{\sigma N}\sigma)^4$ is the nonlinear potential for the scalar field.

The third term in (1) contains the contribution of the Coulomb field (described by the potential $V_{\mathrm{Coul}}(\mathbf{r})$) and the contribution of relativistic electrons,

$$\Omega_e = \int d^3r \left[-\frac{1}{8\pi e^2}(\nabla V_{\mathrm{Coul}})^2 - \frac{(\mu_e - V_{\mathrm{Coul}})^4}{12\pi^2} \right], \quad (5)$$

where μ_e is the electron chemical potential.

The last term in (1) is the thermodynamic potential of the mean K^- meson field,

$$\begin{aligned} \Omega_K &= \int d^3r \left\{ -\frac{f_K^2\theta^2}{2} \left[-{m_K^*}^2 + (\mu_K - V_{\mathrm{Coul}} \right. \right. \\ &\left. \left. + g_{\omega K}\omega_0 + g_{\rho K} R_0)^2 \right] + \frac{f_K^2(\nabla\theta)^2}{2} \right\}, \quad (6) \end{aligned}$$

where $m_K^*(\mathbf{r}) = m_K - g_{\sigma K}\sigma(\mathbf{r})$ is the effective K^- mass, m_K is the kaon mass in vacuum, $g_{\sigma K}$, $g_{\omega K}$, $g_{\rho K}$ are the coupling constants, μ_K is the K^- chemical potential, $K = f_K\theta/\sqrt{2}$ is the kaon field and $f_K \simeq 93$ MeV is the kaon decay constant [69]. The kaon charge density ρ_K is expressed in terms of the kaon field θ as

$$\rho_K = -\left(\mu_K - V_{\mathrm{Coul}} + g_{\omega K}\omega_0 + g_{\rho K} R_0\right) f_K^2\theta^2. \quad (7)$$

Temperature T is kept zero in the present study.

For nucleons and electrons we used the local-density approximation, i.e., nucleons and electrons are described by their local densities. This approximation has its sense only if the typical length of the change of the nucleon density is larger than the inter-nucleon distance. Derivative terms of the particle densities can be incorporated in the quasi-classical manner by the derivative expansion within the density functional theory [54]. Their contribution to the energy can be reduced to a surface tension term. Here we simply discard those derivative terms, as a first-step approximation. Thus we discard the contribution of the nucleon fields to the surface tension assuming that it is smaller than the corresponding contribution of the meson fields that we retain. In the case when we suppress derivative terms of the nucleon densities they follow changes of the meson σ, ω, ρ mean fields and the kaon and the Coulomb fields that have derivative terms. Note that we have fitted our model to properly describe finite nuclei (see below) without including nucleon derivative terms. If we introduced them it would need to re-adjust the model parameters. We should bear in mind that for small structure sizes quantum effects become prominent. For simplicity we disregard these effects. Thus within this scheme we may properly describe only rather large-size structures.

B. Equations of motion and numerical procedure

Equations of motion for the mean fields including kaon and for the Coulomb potential are obtained from the variational principle: $\frac{\delta\Omega}{\delta\phi_i(\mathbf{r})} = 0$ ($\phi_i = \sigma, \omega_0, R_0, \theta, V_{\mathrm{Coul}}$) and $\frac{\delta\Omega}{\delta\rho_a(\mathbf{r})} = 0$ ($a = n, p, e$). These equations read

$$\begin{aligned} \nabla^2\sigma(\mathbf{r}) &= m_\sigma^2\sigma(\mathbf{r}) + \frac{dU}{d\sigma} - g_{\sigma N}(\rho_n^{(s)}(\mathbf{r}) + \rho_p^{(s)}(\mathbf{r})) \\ &\quad + 2g_{\sigma K} m_K f_K^2\theta^2(\mathbf{r}), \quad (8) \\ \nabla^2\omega_0(\mathbf{r}) &= m_\omega^2\omega_0(\mathbf{r}) - g_{\omega N}(\rho_p(\mathbf{r}) + \rho_n(\mathbf{r})) \\ &\quad - f_K^2 g_{\omega K}\theta^2(\mathbf{r})(\mu_K - V_{\mathrm{Coul}}(\mathbf{r}) \\ &\quad + g_{\omega K}\omega_0(\mathbf{r}) + g_{\rho K} R_0(\mathbf{r})), \quad (9) \\ \nabla^2 R_0(\mathbf{r}) &= m_\rho^2 R_0(\mathbf{r}) - g_{\rho N}(\rho_p(\mathbf{r}) - \rho_n(\mathbf{r})) \\ &\quad - f_K^2 g_{\rho K}\theta^2(\mathbf{r})(\mu_K - V_{\mathrm{Coul}}(\mathbf{r}) \\ &\quad + g_{\omega K}\omega_0(\mathbf{r}) + g_{\rho K} R_0(\mathbf{r})), \quad (10) \\ \nabla^2\theta(\mathbf{r}) &= \left[m_K^*(\mathbf{r})^2 - (\mu_K - V_{\mathrm{Coul}}(\mathbf{r}) \right. \\ &\quad \left. + g_{\omega K}\omega_0(\mathbf{r}) + g_{\rho K} R_0(\mathbf{r}))^2 \right]\theta(\mathbf{r}), \quad (11) \\ \nabla^2 V_{\mathrm{Coul}}(\mathbf{r}) &= 4\pi e^2 \rho_{\mathrm{ch}}(\mathbf{r}), \quad (12) \end{aligned}$$

the charge density $\rho_{\mathrm{ch}}(\mathbf{r}) = \rho_p(\mathbf{r}) + \rho_e(\mathbf{r}) + \rho_K(\mathbf{r})$,

$$\begin{aligned} \mu_n &= \mu_B = \sqrt{k_{Fn}(\mathbf{r})^2 + m_N^*(\mathbf{r})^2} \\ &\quad + g_{\omega N}\omega_0(\mathbf{r}) - g_{\rho N} R_0(\mathbf{r}), \quad (13) \\ \mu_p &= \mu_B - \mu_e = \sqrt{k_{Fp}(\mathbf{r})^2 + m_N^*(\mathbf{r})^2} \end{aligned}$$

TABLE I: Parameter set used in RMF in our calculation.

$g_{\sigma N}$	$g_{\omega N}$	$g_{\rho N}$	b	c	m_σ	m_ω	m_ρ	$f_K(\approx f_\pi)$	m_K	$g_{\omega K}$	$g_{\rho K}$	$U_K(\rho_0)$
6.3935	8.7207	4.2696	0.008659	0.002421	400 MeV	783 MeV	769 MeV	93 MeV	494 MeV	$g_{\omega N}/3$	$g_{\rho N}$	-120 – -130 MeV

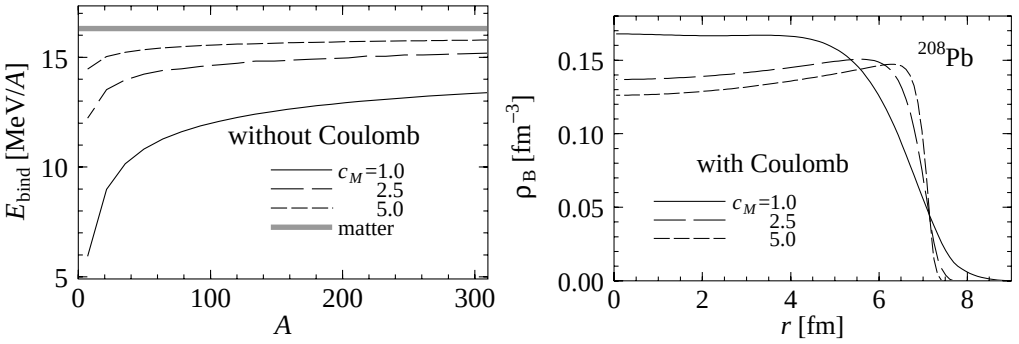

FIG. 1: The mass number A dependence of the binding energy of finite nuclei (left) and the density profile of ^{208}Pb nucleus (right). Different curves correspond to different meson masses used in the RMF calculation. Thick horizontal gray line in the left panel shows the case of the nuclear matter for the comparison.

$$+ g_{\omega N}\omega_0(\mathbf{r}) + g_{\rho N}R_0(\mathbf{r}) - V_{\rm Coul}(\mathbf{r}). \tag{14}$$

The last two equations are the standard relations between the local nucleon densities and chemical potentials. We have assumed that the system is in the chemical equilibrium in respect to the weak, electromagnetic and strong interactions and we introduced the baryon chemical potential $\mu_B = \mu_n$ and the charge chemical potential, i.e. the electron chemical potential, μ_e, according to the corresponding conserved charges. Under the same assumption $\mu_K = \mu_e$.

To solve the above coupled equations numerically, the whole space is divided into equivalent Wigner-Seitz cells. The geometrical shape of the cell changes as follows: sphere in three-dimensional (3D) calculation, cylinder in 2D and slab in 1D, respectively. Each cell is globally charge-neutral and all physical quantities in the cell are smoothly connected to those of the next cell with zero gradients at the boundary. Every point inside the cell is represented by the grid points (number of grid points $N_{\rm grid} \approx 100$) and differential equations for fields are solved by the relaxation method for a given baryon-number density under constraints of the global charge neutrality. Details of the numerical procedure are explained in Ref. [49].

C. Parameter set and finite nuclei

For the study of a non-uniform nuclear matter, the ability to reproduce the bulk properties of finite nuclei should be essential. Parameters of the RMF model are chosen to reproduce saturation properties of nuclear matter: the minimum energy per nucleon -16.3 MeV at $\rho = \rho_0 \equiv 0.153$ fm^{-3}, the incompressibility $K(\rho_0) = 240$ MeV, the effective nucleon mass $m_N^*(\rho_0) = 0.78 m_N$; $m_N = 938$ MeV, and the isospin-asymmetry coefficient $a_{\rm sym} = 32.5$ MeV. Coupling constants and meson masses used in our calculation are listed in Table I.

The parameter $g_{\sigma K}$ enters the value of the K^- optical potential U_K defined by $U_K = g_{\sigma K}\sigma + g_{\omega K}\omega_0$. There have been many works trying to fix U_K at the saturation density from the data on the kaonic atoms [55, 56] and from calculations [57, 58, 59, 60, 61], but there is still a controversy in its depth. We take here a somewhat deep potential, as shown in Table I, to compare our results with the previous ones [23, 24, 25, 26]. To understand a dependence of the results on the value U_K we further allow for a variation of it.

We have checked that with the meson masses listed in Table I ($m_\sigma = 400$ MeV, etc.) and by including the Coulomb interaction, the binding energies of finite nuclei and the proton fraction, as well as the nucleon density profiles are well reproduced, except for very light nuclei [49].

We examine in this section how the surface tension could be correctly incorporated in our RMF calculation. We explicitly treat the kaon gradient term in (11) since, as we show, the kaon and Coulomb fields are essentially coupled and due to that the scales of changes of these fields prove to be of the same order of magnitude. These are long scales. Reference [62] using an analytical model describing the charge distribution in a pion condensate droplet has demonstrated that actually there exists only one long scale in the problem. Namely due to that one

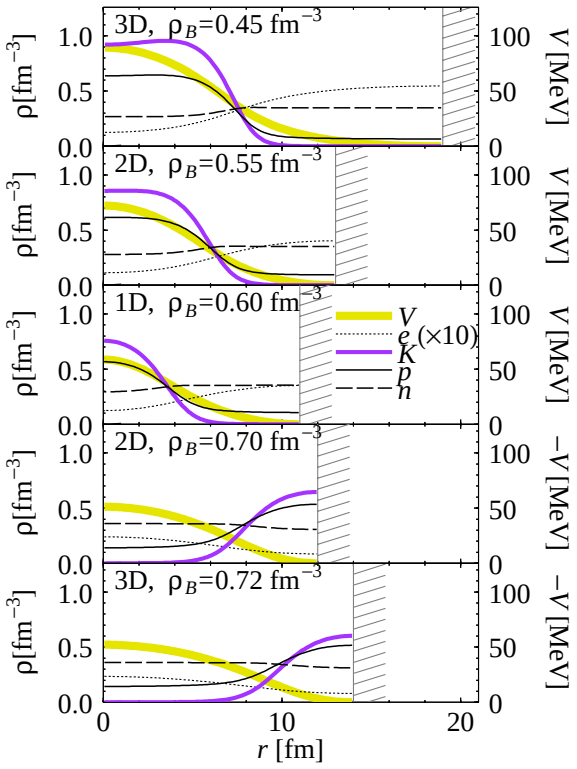

FIG. 2: (Color online) Density profiles of kaonic structures. Here the density does not mean charge-density but number-density of particles. U_k, the kaon optical potential at the nuclear saturation density, is set to be -130 MeV. Displayed using the right axis is the Coulomb potential $V_{\rm Coul}$ (written as "V").

cannot reduce the kaon contribution to a purely surface term in case the Coulomb interaction is introduced in equations of motion.

On the other hand the σ, ω, ρ prove to be short-range fields. In order to test effects of gradient terms of the short-range meson fields in (4) and (8)–(10) we multiply meson masses m_σ, m_ω and m_ρ by a factor c_M. We take $c_M = 1$ (in realistic case), 2.5 and 5.0. For example, with the factor $c_M = 2.5$ we get the choice m_σ=1000 MeV, m_ω=1958 MeV and m_ρ=1923 MeV. However to obtain appropriate matter properties, we simultaneously fix the ratio $g^2_{\phi N}/m^2_\phi$ (ϕ=σ, ω and ρ) for all values of m_ϕ because thermodynamic characteristics depend only on $g^2_{\phi N}/m^2_\phi$ rather than on $g_{\phi N}$ and m_ϕ separately.

First to show the effect of thus simulated surface tension we discard the Coulomb interaction (except that we use the global charge neutrality condition). Left panel of Fig. 1 demonstrates the binding energy of finite nuclei calculated with different meson masses. We have checked that for all sets of σ, ω, ρ meson masses (for different c_M) the curves approach the value of the binding energy of the nuclear matter for $A \to \infty$. Also by the use of heavy meson masses, the binding energy of finite nuclei (for finite A) approaches to that of nuclear matter indicated by a thick gray line. This shows that the surface tension is reduced with the increase of the meson masses, cf. [63]. Notice that this statement is correct only if we fixed the ratio $g^2_{\phi N}/m^2_\phi$.

Then we allow for the Coulomb interaction. Right panel of Fig. 1 shows the baryon density profile of ^{208}Pb nucleus obtained with different c_M factors. With a larger c_M, i.e. with a weaker surface tension, the baryon density at the center decreases and that near the surface increases due to the Coulomb repulsion of protons.

When we further discuss the kaonic pasta structures in the later section, we compare results obtained with standard meson masses and those with heavy meson masses to figure out the effect of the surface tension due to the meson mean-fields.

III. RESULTS

The density profile is determined by solving equations of motion (8)–(14). For each baryon density, the cell radius and the geometrical dimension are chosen to minimize the energy. If Glendenning's claim were correct, the structured mixed phase would develop in a broad density range from well below to well above the critical densities determined by the Maxwell construction. In this density interval the matter should exhibit the structure change, similar to the nuclear "pasta" phases [49]: the kaonic droplet, rod, slab, tube, bubble. We observe such structures in our calculation as well.

Figure 2 displays typical density profiles and the Coulomb potential. The horizontal axis is the distance from the cell center and the hatch shows the cell boundary. The symbols "3D" (three dimensional) etc. indicate the dimensionality of the geometry. From the top of the figure, the matter structures correspond to kaonic droplet, rod, slab, tube, and bubble. The neutron distribution proves to be rather flat. The Coulomb potential is given by imposing the gauge condition. Here we fix the gauge by the condition, $V_{\rm Coul}(R_{\rm cell}) = 0$ for all the cases. Note that the maximum value of the Coulomb potential becomes rather large.

In the upper panel of Fig. 3 we depict the energy per nucleon of the matter. The dotted line indicates the case of single phase (if one assumes absence of the mixed phase). In this case the uniform matter consists of normal nuclear matter for undercritical densities and the kaonic matter for overcritical densities. The cross on the dotted line ($\rho_B \simeq 0.46$ fm^{-3}) shows the critical density, i.e. the point where kaons begin to condensate in the case of single phase. Pieces of solid curves, on the other hand, indicate energetically favored structures. Droplets begin to appear for $\rho_B > 0.41$ fm^{-3} smoothly decreasing the energy of the system. The mixed phase disappears for $\rho_B > 0.74$ fm^{-3}. The occurrence of the kaonic pasta structures, i.e. kaonic droplet, rod, slab, tube, and bubble, results in a softening of the matter (the energy decreases with their appearance).

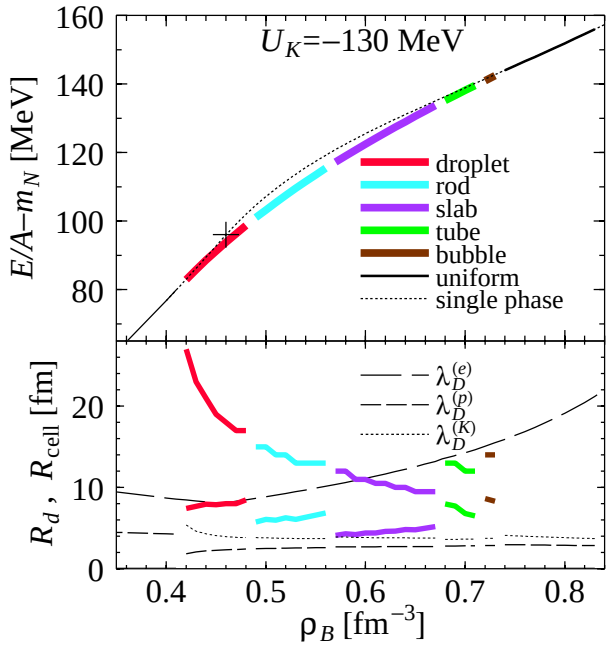

FIG. 3: (Color online) Top: Binding energy per nucleon of the nuclear matter in the beta equilibrium. The dotted line below the cross shows the uniform normal nuclear matter and above the cross, the uniform kaonic matter. Bottom: Structure size R_d (thick curves below) and cell size $R_{\rm cell}$ (thick curves above). Compared are the Debye screening lengths of electron, proton and kaon. The Debye screening lengths are calculated using the explicit dependence of μ_a on ρ_a.

In the lower panel of Fig. 3 we plot the structure sizes (for droplet, rod, slab, tube and bubble) R_d and the corresponding cell sizes $R_{\rm cell}$. The structure size R_d is calculated by the use of the averaged density and its spacial fluctuation as in Ref. [49]. We find that at the onset density the radius of the cell is infinitely large in case of the full calculation. The corresponding steep increase of $R_{\rm cell}$ with decreasing density is clearly seen in the figure.

To roughly estimate the Debye screening length $\lambda_D^{(a)}$ (see Appendix B for detail) let us for simplicity use only explicit dependence of $\langle\rho_a\rangle$ on μ_a in (B3), i.e., let us replace $\dfrac{d\langle\rho_a\rangle}{d\mu_a}$ by $\dfrac{\partial\langle\rho_a\rangle}{\partial\mu_a}$, hence $\dfrac{\partial\langle\rho_e\rangle}{\partial\mu_e} \approx -\dfrac{\mu_e^2}{\pi^2}$, $\dfrac{\partial\langle\rho_p\rangle}{\partial\mu_p} \approx \dfrac{\langle k_{Fp}\rangle\sqrt{\langle k_{Fp}\rangle^2+{m_N}^2}}{\pi^2}$ for electron and proton, and $\dfrac{\partial\langle\rho_K\rangle}{\partial\mu_K} \approx \langle -f^2\theta^2\rangle$ for kaon. Here, the bracket "$\langle ...\rangle$" indicates an averaging over an appropriate region (cf. Appendix B). The dashed lines and the dotted line in the lower panel of Fig. 3 show thus treated partial contributions to the Debye screening lengths of the electron, proton and kaon, $\lambda_D^{(e)}$, $\lambda_D^{(p)}$, and $\lambda_D^{(K)}$, respectively. We see that in most cases $\lambda_D^{(e)}$ is less than the cell size $R_{\rm cell}$ but it is larger than the structure size R_d. The proton Debye length $\lambda_D^{(p)}$ and the kaon Debye length $\lambda_D^{(K)}$, on the other hand, are always shorter than $R_{\rm cell}$ and the structure size R_d. Now we are able to estimate the value of the resulting total Debye screening length $\lambda_D^{(\rm tot)}$. For example in the case of $\rho_B = 0.55$ fm^{-3} we obtain $\lambda_D^{(\rm tot)} \simeq 3$ fm.

On the other hand the typical length of the Coulomb potential is ~ 5 fm for $\rho_B = 0.55$ fm^{-3} (see Fig. 2). This value is longer than the above estimated Debye screening length due to the implicit dependence of ρ_a on μ_a.

From this comparison we conclude that a consistent inclusion of the Coulomb screening effect is not a trivial problem and it has really important consequences for the correct description of density profiles of protons and kaons (see Fig. 7 below).

So far we have presented results for the K^- optical potential in nucleus equal to $U_K = -130$ MeV. With a lower value $U_K = -120$ MeV, the density range of the kaonic pasta is narrowed: from $\rho_B = 0.49$ to 0.71 fm^{-3} instead of from $\rho_B = 0.41$ to 0.74 fm^{-3} in the case of $U_K = -130$ MeV. The effect of the kaon pasta structures on the EOS (the energy difference between single phase calculation and full calculation) becomes still smaller. The kaon and proton densities in a droplet become $20-30$ % lower than those for the case $U_K = -130$ MeV, and the neutron density increases. Other features remain qualitatively the same.

IV. CHARGE SCREENING AND SURFACE EFFECTS

A. Charge screening effect

To demonstrate the charge screening effects we compare our results with those given by a "perturbative" treatment of the Coulomb interaction often used in the literature, "no Coulomb" calculation (see Appendix A for details). The electric potential is discarded in equations of motion (7)–(11), (13), (14) which determine the density profiles. The Coulomb energy is then added to the total energy by using the charge density profile thus determined to find the optimal value with respect to the cell size $R_{\rm cell}$. Comparing Figs. 3 and 4, we see that the density range of the mixed phase is more narrow in the case of the "no Coulomb" calculation than in the full calculation, while the energy gain is almost the same. A remarkable difference is seen in the cell radii, especially near the onset density of kaonic pastas, for $\rho_B < 0.5$ fm^{-3}. The cell size given by the full calculation is always larger than that given by the "no Coulomb" calculation.

To elucidate the screening effect, we depict the $R_{\rm cell}$ dependence of the energy per nucleon in Fig. 5 in both cases. In the full calculation a large cell with a small volume fraction $f \equiv (R_d/R_{\rm cell})^3$ appears near the onset density, which situation is close to the uniform single phase. On the other hand, a smaller cell appears near the onset density in the "no Coulomb" calculation. The energy gain is higher in the full calculation. The cell

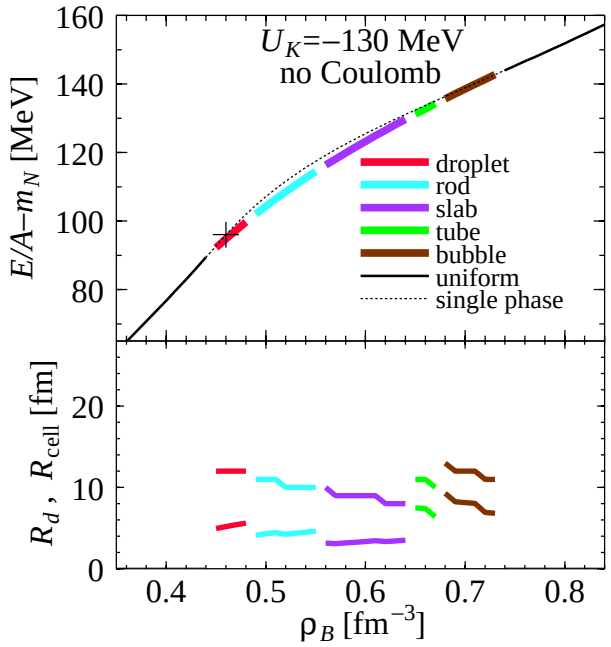

FIG. 4: (Color online) Top: the binding energy per nucleon of the nuclear matter in beta equilibrium. The electric potential is discarded determining the density profile and added evaluating the energy. Bottom: the structure size R_d (thick curves below) and the cell size $R_{\rm cell}$ (thick curves above).

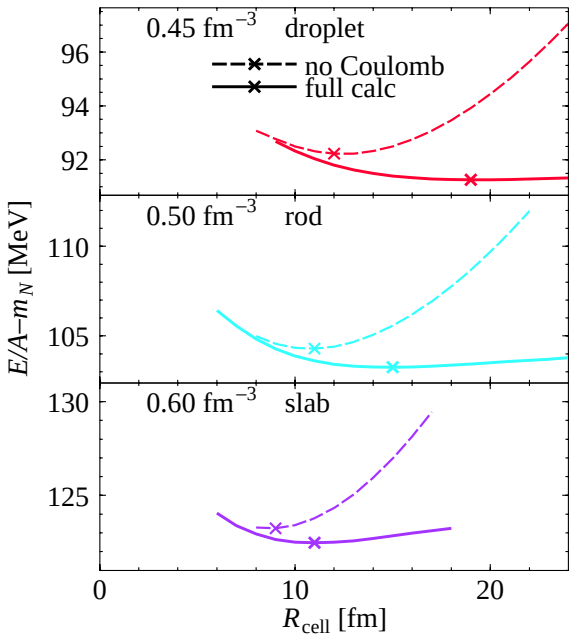

FIG. 5: (Color online) The cell size $R_{\rm cell}$ dependence of the energy per nucleon. Crosses on the curves indicate the minimum points.

radii obtained in both calculations deviate essentially for droplets, less for rods, still less for slabs, etc.

The differences of both calculations are also seen from Fig. 6, where we present the pressure as a function of the baryon-number density. In the case of the full calculation the pressure changes continuously. In the case of the "no Coulomb" calculation there arises a jump in the pressure at the onset density at which the droplets begin to appear. The pressure jump clearly shows that a large structure change occurs at the onset density. The discontinuity arises as an artifact of the "no Coulomb" calculation. The Coulomb energy is overestimated in this case for large values of $R_{\rm cell}$, compared to that for the full calculation, where occurs the screening effect. Indeed, the Coulomb energy per droplet grows proportionally to $R_{\rm cell}^2$ in the case of the "no Coulomb" calculation since the bare Coulomb interaction has an infinite range. On the other hand in the full calculation there appears another length scale, the Debye screening length, and thereby the screened Coulomb interaction is no longer scale-invariant. Thus when the structure radius is significantly larger than the minimal screening length the Coulomb energy contribution becomes ineffective.

In Fig. 6, we also depict the pressure when the Gibbs conditions are applied for two semi-infinite matters disregarding the Coulomb interaction (indicated by "Gibbs") and that given by the Maxwell construction (indicated by "Maxwell"). We see that the pieces of solid curves lie between "Gibbs" and "Maxwell". The full calculation case is more similar to the one given by the Maxwell construction.

To further demonstrate the charge screening effect on the kaonic pasta, We compare the density profiles obtained by the full and "no Coulomb" calculations in Fig. 7. In case of the full calculation the difference between the negative charge density (of kaons and electrons) and the positive charge density of protons is smaller, demonstrating that the profiles are more close to those given by the local charge neutrality. These results also suggest that the Maxwell construction is effectively justified in the full calculation case owing to the charge screening effects. Also we see that the absolute value of the kaon charge density is substantially larger in the "no Coulomb" case. This gives us an additional argument for the essential coupling of the kaon and Poisson equations. Modification of the Coulomb term in the kaon equation significantly affects the charged kaon distribution whereas changes in the proton, neutron and electron distributions are more smooth.

B. Surface effects

Next we investigate the effect of the surface tension caused by the meson mean-fields on the kaonic pasta structures. The previous calculation by Norsen and Reddy [26, 53] was done discarding the gradient terms of σ, ω and ρ mesons. The calculation with infinitely heavy meson masses would correspond to it.

Figure 8 shows the same quantities as Fig. 3, EOS and

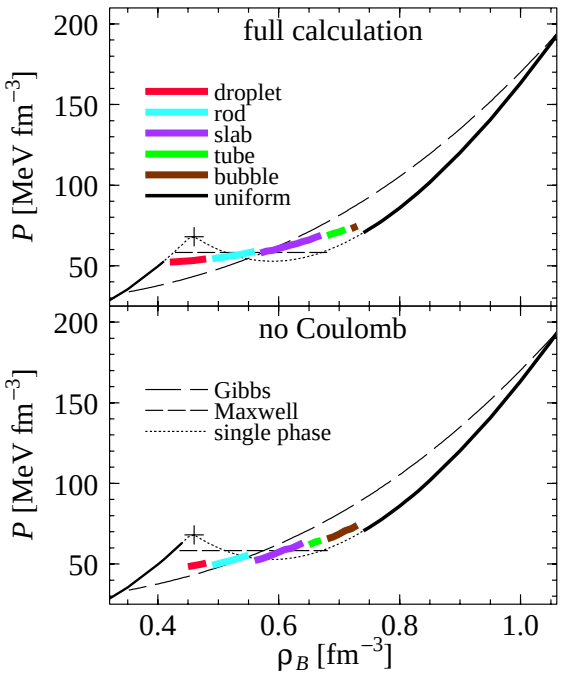

FIG. 6: (Color online) The pressure versus the baryon number density.

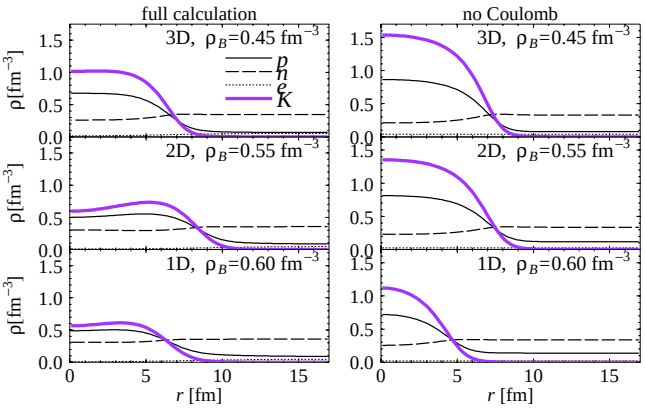

FIG. 7: (Color online) Comparison of density profiles of kaonic matter in full calculation and in "no Coulomb" case. The cell size, $R_{\rm cell} = 17$ fm, is not optimized since the optimum values would be different for different treatments of the Coulomb interaction.

the structure size, but now for the case of an artificially suppressed surface tension (for $c_M = 5.0$). Comparing Figs. 8 and 3, we see that there is almost no difference in the EOS. However, the density range of pasta structure is slightly broader for the case of the weaker surface tension. The reason for a similarity of Figs. 8 and 3 is as follows: Even without the contribution of gradient terms of σ, ω and ρ mesons (that corresponds to infinitely massive mesons, however for fixed $g^2_{\phi N}/m^2_\phi$), there is still a contribution from the kaon gradient term in Eq. (6). In our case the kaon and the Coulomb fields have similar typical length scales. The Coulomb term is mainly balanced by the kaon term, and the structure size is actually determined by the minimum of the Coulomb plus kaon kinetic energy. The pasta structure is realized by the balance between the surface tension and the Coulomb repulsion. In this sense, σ, ω and ρ mesons have less contribution to the surface tension compared to kaon in the case of kaonic pasta structure, although the clear distinction of the Coulomb repulsion and the surface tension is difficult due to the screening effects and the large surface diffuseness.

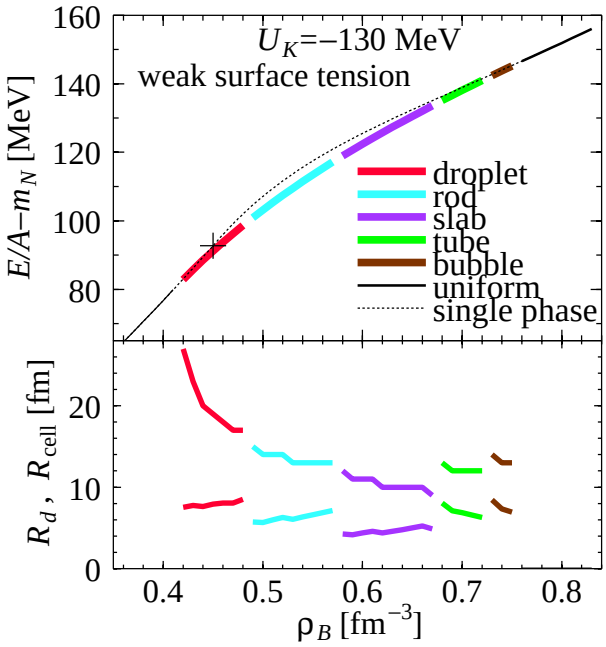

FIG. 8: (Color online) Top: Binding energy per nucleon of the nuclear matter in beta equilibrium. Bottom: Structure size R_d (thick curves below) and the cell size $R_{\rm cell}$ (thick curves above).

V. SUMMARY AND CONCLUDING REMARKS

We have discussed the effects of the charge screening and the surface tension on the kaonic pasta. Since the kaon mixed-phase appears at high-densities, we see that changes are more remarkable than for the "nuclear pasta" at subnuclear densities [48]. We found that the density range of the structured mixed phase is largely limited by the charge screening and thereby the phase diagram becomes similar to that given by the Maxwell construction. Although the importance of such a treatment has been demonstrated for the hadron-quark matter transition [6, 9], one of our new findings here is that we can figure out the role of the charge screening effect without introducing any "artificial" input of the surface-tension parameter. For this aim in our study we have used the relativistic mean field approach.

On the other hand we remind that the bulk calculation, where finite size effects (the Coulomb interaction and the surface tension) are not included, does not produce the mixed phase in the chiral models [21, 27, 52]. Thus it should be interesting to perform the same self-consistent study with properly included finite size effects, as we have done above, but within a chiral model.

In application to the newly formed neutron stars in supernova explosions, finite temperature and neutrino trapping effects become important, as well as the dynamics of the first order phase transition with formation of the structures. It would be interesting to extend our framework to include these effects.

We focused our study on the s-wave kaon condensation. However it would be interesting to extend it to the possibility of the p-wave kaon condensation.

It might be also interesting to apply our framework to the problem of kaonic nuclei [64, 65, 66, 67], similar to the description of finite nuclei. Within our framework we can construct a consistent description of kaonic nuclei by taking into account the Coulomb interaction as well as the KN interaction [68].

Acknowledgments

We thank S. Reddy for discussions and communications. This work is partially supported by the Grant-in-Aid for the 21st Century COE "Center for the Diversity and Universality in Physics" from the Ministry of Education, Culture, Sports, Science and Technology of Japan. It is also partially supported by the Japanese Grant-in-Aid for Scientific Research Fund of the Ministry of Education, Culture, Sports, Science and Technology (13640282, 16540246). The work of D.N.V. was also supported in part by the Deutsche Forschungsgemeinschaft (DFG project 436 RUS 113/558/0-2).

APPENDIX A: "NO COULOMB" CALCULATION

We briefly describe here the "no Coulomb" approximation, which has been frequently used in the bulk calculations. To begin with we present the thermodynamic potential (1) as

$$\Omega(V_{\rm Coul}) = \Omega_{\rm matter}(V_{\rm Coul}) - \int d^3r \frac{1}{8\pi e^2}(\nabla V_{\rm Coul})^2, \tag{A1}$$

where we isolated the electric field contribution and $\Omega_{\rm matter}(V_{\rm Coul})$ summarizes other baryon, electron, kaon and mean-field contributions. Expanding $\Omega(V_{\rm Coul})$ around a reference value $V_{\rm Coul} = V_0 = const.$ we have

$$\begin{aligned}\Omega(V_{\rm Coul}) &= \Omega_{\rm matter}(V_0) \\ &+ \int d^3r \left.\frac{\delta\Omega_{\rm matter}(V_{\rm Coul})}{\delta V_{\rm Coul}(r)}\right|_{V_0} (V_{\rm Coul}(r) - V_0) \\ &- \int d^3r \frac{(\nabla V_{\rm Coul})^2}{8\pi e^2} + O\left[(V_{\rm Coul}(r) - V_0)^2\right]. \end{aligned} \tag{A2}$$

The non-zero value of V_0 shifts the value of the charge chemical potential in such a way that only the combination $\mu - V_{\rm Coul} + V_0$ is meaningful due to the gauge invariance. To be specific in the paper body we performed calculations in the "no Coulomb" case with $V_0 = 0$. Since $\Omega_{\rm matter}(V_{\rm Coul})$ includes $V_{\rm Coul}$ in a gauge invariant way, it can be further rewritten as

$$\begin{aligned}\Omega(V_{\rm Coul}) &= \Omega_{\rm matter}(V_0) - \int d^3r \rho^{\rm ch}(V_0)\,(V_{\rm Coul}(r) - V_0) \\ &- \int d^3r \frac{(\nabla V_{\rm Coul})^2}{8\pi e^2} + O\left((V_{\rm Coul}(r) - V_0)^2\right). \end{aligned} \tag{A3}$$

Using the total charge neutrality condition, it eventually reads

$$\Omega(V_{\rm Coul}) \equiv \Omega^{\rm NC}(V_{\rm Coul}) + O\left((V_{\rm Coul}(r) - V_0)^2\right), \tag{A4}$$

with

$$\begin{aligned}\Omega^{\rm NC}(V_{\rm Coul}) &= \Omega_{\rm matter}(V_0) - \int d^3r \rho^{\rm ch}(V_0) V_{\rm Coul}(r) \\ &- \int d^3r \frac{(\nabla V_{\rm Coul})^2}{8\pi e^2}. \end{aligned} \tag{A5}$$

The Poisson equation for $V_{\rm Coul}$ is given by

$$\nabla^2 V_{\rm Coul} = 4\pi e^2 \rho^{\rm ch}(V_0), \tag{A6}$$

while the equations of motion for other fields and density profiles, $f_\alpha(\mathbf{r}) \equiv \phi_i(\mathbf{r}), \rho_a(\mathbf{r})$, read

$$\frac{\delta\Omega_{\rm matter}(V_0)}{\delta f_\alpha(\mathbf{r})} - \frac{\partial\rho^{\rm ch}(V_0)}{\partial f_\alpha(\mathbf{r})} V_{\rm Coul}(r) = 0. \tag{A7}$$

In (A7) one can neglect the second term of the electromagnetic origin compared to the first term related to the strong interaction. Then one has

$$\frac{\delta\Omega_{\rm matter}(V_0)}{\delta f_\alpha(\mathbf{r})} \simeq 0, \tag{A8}$$

Using Eq. (A6), we can recast Eq. (A5) into the form,

$$\begin{aligned}\Omega^{\rm NC}(V_{\rm Coul}) &= \Omega_{\rm matter}(V_0) - \frac{1}{2}\int d^3r \rho^{\rm ch}(V_0) V_{\rm Coul}(r) \\ &= \Omega_{\rm matter}(V_0) + \int d^3r \frac{(\nabla V_{\rm Coul})^2}{8\pi e^2}. \end{aligned} \tag{A9}$$

Equations (A6), (A8) and (A9) are used in the "no Coulomb" calculation. The second term in Eq. (A9) (let's call it the Coulomb energy) gives a positive (repulsive) contribution.

The corresponding total energy $E^{\rm NC}$ is then given by the Legendre transformation from $\Omega^{\rm NC}$,

$$E^{\rm NC} = \Omega^{\rm NC} + \mu_B \sum_{a=n,p} \int d^3r \rho_a \tag{A10}$$

with

$$\rho_a = \frac{\partial \Omega_{\rm matter}(V_0)}{\partial \mu_a}. \qquad \text{(A11)}$$

In order to proceed beyond the "no Coulomb" approximation one should perform the expansion in (A2) at least including the quadratic terms. With these terms one arrives at the linearized Poisson equation for the Coulomb potential that incorporates the Debye screening, cf. [6, 7].

APPENDIX B: DEBYE SCREENING LENGTH

To roughly estimate the screening effect we can introduce the Debye screening lengths as follows. A linearized Poisson equation for the Coulomb potential $\delta V_{\rm Coul} = V_{\rm Coul} - \mu_e - V_0$, where V_0 is the reference constant value, takes the form [70]

$$\Delta \delta V_{\rm Coul} + \left(\lambda_D^{(\rm tot)}\right)^{-2} \delta V_{\rm Coul} = 0, \qquad \text{(B1)}$$

$$\left(\lambda_D^{(\rm tot)}\right)^{-2} = \sum_{a=e,p,K} \left(\lambda_D^{(a)}\right)^{-2}, \qquad \text{(B2)}$$

$$\lambda_D^{(a)} = \left(4\pi e^2 \frac{d\,|\langle \rho_a \rangle|}{d\mu_a}\right)^{-1/2}. \qquad \text{(B3)}$$

The partial contributions $\lambda_D^{(a)}$, the Debye screening lengths, are dependent on the region. To find typical values characterized screening inside the structure we average ρ_a over the region where the relevant charge density is non-zero. Thus the averaging region for proton and kaon is inside the lump and that for electron is the cell.

To obtain correct values of the Debye screening lengths, the implicit dependence of $\langle \rho_a \rangle$ on μ_a through the change of mean fields and the Coulomb potential should be taken into account. We will see that it is especially in the case of the kaon Debye term. Indeed, the linearization procedure should be performed in all fields and the linearized Poisson equation is as follows:

$$\begin{aligned} &\Delta \delta V_{\rm Coul} + a_{VV} \delta V_{\rm Coul} + a_{V\sigma} \delta\sigma \qquad \text{(B4)} \\ &+ a_{V\omega} \delta\omega_0 + a_{V\rho} \delta R_0 + a_{V\theta} \delta\theta \\ &+ a_{Vn} \delta\rho_n + a_{Vp} \delta\rho_p = 0, \end{aligned}$$

where a_{Vi} are density dependent coefficients. The fields $\delta\sigma$, $\delta\omega_0$, δR_0, $\delta\theta$ are determined by their own equations of motion having similar forms. Also variation of equations for μ_n and μ_p yields equations for $\delta\rho_n$ and $\delta\rho_p$, μ_e is unambiguously expressed via the neutron and proton chemical potentials, therefore we did not present the corresponding term in (B4). Neglecting derivative terms for all the fields except for the Coulomb field in the system of equations similar to (B4) one can express $\delta\sigma$, $\delta\omega_0$, δR_0, $\delta\rho_n$ and $\delta\rho_p$ as functions of the only one $\delta V_{\rm Coul}$ variable and one finally arrives at Eq. (B1). However such a procedure is legitimate only for short-scale fields, $\delta\sigma$, $\delta\omega_0$, δR_0, $\delta\rho_n$ and $\delta\rho_p$ but not for the kaon field $\delta\theta$ since the later field proves to be a long-scale field. The value $\Delta\delta\theta$ entering the kaon equation of motion cannot be omitted thereby.

[1] C. B. Das, S. das Gupta, W. G. Lynch, A. Z. Mekjian and M. B. Tsang, Phys. Rept. **406**, 1 (2005).
[2] A. B. Migdal, E.E. Saperstein, M. A. Troitsky, and D. N. Voskresensky, Phys. Rept. 192, 179 (1990).
[3] N. K. Glendenning, Phys. Rev. **D46**, 1274 (1992); N. K. Glendenning, Phys. Rep. **342**, 393 (2001).
[4] H. Heiselberg, C. J. Pethick and E. F. Staubo, Phys. Rev. Lett. **70**, 1355 (1993).
[5] N. K. Glendenning and S. Pei, Phys. Rev. **C52**, 2250 (1995).
[6] D. N. Voskresensky, M. Yasuhira and T. Tatsumi, Phys. Lett. **B541**, 93 (2002);
T. Tatsumi and D. N. Voskresensky, nucl-th/0312114.
[7] D. N. Voskresensky, M. Yasuhira and T. Tatsumi, Nucl. Phys. **A723**, 291 (2003).
[8] T. Tatsumi, T. Maruyama, V. N. Voskresensky, T. Tanigawa and S. Chiba, nucl-th/0502040.
[9] T. Endo, T. Maruyama, S. Chiba and T. Tatsumi, nucl-th/0410102; hep-ph/0502216.
[10] M. Alford, K. Rajagopal, S. Reddy and F. Wilczek, Phys. Rev. **D64**, 074017 (2001).
[11] P. F. Bedaque, Nucl. Phys. **A697**, 569 (2002).
[12] S. Reddy and G. Rupak, nucl-th/0405054.
[13] P. F. Bedaque, H. Caldas and G. Rupak, Phys. Rev. Lett. **91**, 247002 (2003).
[14] T. Tatsumi, E. Nakano and K. Nawa, hep-ph/0506002.
[15] D. N. Voskresensky, Phys. Lett. **B392**, 262 (1997).
[16] E. E. Kolomeitsev and D. N. Voskresensky, Nucl. Phys. **A759**, 373 (2005).
[17] D. Kaplan and A. Nelson, Phys. Lett. **B175**, 57 (1986).
[18] G. E. Brown, C. H. Lee, M. Rho and V. Thorsson, Nucl. Phys. **A567**, 937 (1994).
[19] T. Muto, R. Tamagaki and T. Tatsumi, Prog. Theor. Phys. Suppl. **112**, 159 (1993).
[20] T. Tatsumi, Prog. Theor. Phys. Suppl, **120**, 111 (1995).
[21] J. A. Pons, S. Reddy, P. J. Ellis, M. Prakash and J. M. Lattimer, Phys. Rev. C **62**, 035803 (2000).
[22] S. Reddy, G. F. Bertsch and M. Prakash, Phys. Lett. **B475**, 1 (2000).
[23] N. K. Glendenning and J. Schaffner-Bielich, Phys. Rev. C **60**, 025803 (1999).
[24] M. Christiansen and N. K. Glendenning, astro-ph/0008207.
[25] M. Christiansen, N. K. Glendenning and J. Schaffner-Bielich, Phys. Rev. **C62**, 025804 (2000).
[26] T. Norsen and S. Reddy, Phys. Rev. **C63**, 065804 (2001).
[27] T. Tatsumi and M. Yasuhira, Nucl. Phys. **A653**, 133 (1999);
M. Yasuhira and T. Tatsumi, Nucl. Phys. **A690**, 769 (2001).

[28] E. E. Kolomeitsev, D. N. Voskresensky and B. Kämpfer, Nucl. Phys. **A588** (1995) 889;
E. E. Kolomeitsev and D. N. Voskresensky, Phys. Rev. C **68**, 015803 (2003).

[29] T. Muto, Prog. Theor. Phys. **89**, 415 (1993);
T. Muto, Nucl. Phys. **A697**, 225 (2002) ; Nucl. Phys. **A754**, 350 (2004).

[30] C. H. Lee, Phys. Rep. **275**, 197 (1996).

[31] M. Prakash, I. Bombaci, M. Prakash, P. J. Ellis, J. M. Lattimer, R. Knorren, Phys. Rep. **280**, 1 (1997).

[32] G. E. Brown and H. A. Bethe, Astrophys. J. **423**, 659 (1994).

[33] G. E. Brown, K. Kubodera, D. Page and P. Pizzecherro, Phys. Rev. **D37**, 2042 (1988).

[34] T. Tatsumi, Prog. Theor. Phys. **80**, 22 (1988).

[35] H. Fujii, T. Muto, T. Tatsumi and R. Tamagaki, Nucl. Phys. **A571**, 758 (1994); Phys. Rev. **C50**, 3140 (1994).

[36] D. Page and E. Baron, Astrophys. J. **254**, L17 (1990).

[37] D. G. Ravenhall, C. J. Pethick and J. R. Wilson, Phys. Rev. Lett. **50**, 2066 (1983).

[38] M. Hashimoto, H. Seki and M. Yamada, Prog. Theor. Phys. **71**, 320 (1984).

[39] R. D. Williams and S. E. Koonin, Nucl. Phys. **A435**, 844 (1985).

[40] K. Oyamatsu, Nucl. Phys. **A561**, 431 (1993).

[41] C. P. Lorentz, D. G. Ravenhall and C. J. Pethick, Phys. Rev. Lett. **70**, 379 (1993).

[42] K. S. Cheng, C. C. Yao and Z. G. Dai, Phys. Rev. **C55**, 2092 (1997).

[43] T. Maruyama, K. Niita, K. Oyamatsu, Tomoyuki Maruyama, S. Chiba and A. Iwamoto, Phys. Rev. **C57**, 655 (1998).

[44] T. Kido, T. Maruyama, K. Niita and S. Chiba, Nucl. Phys. **A663-664**, 877 (2000).

[45] G. Watanabe, K. Iida and K. Sato, Nucl. Phys. **A676**, 445 (2000);

[46] G. Watanabe, K. Sato, K. Yasuoka and T. Ebisuzaki, Phys. Rev. **C66**, 012801 (2002).

[47] G. Watanabe and K. Iida, Phys. Rev. **C68**, 045801 (2003).

[48] T. Maruyama, T. Tatsumi, V. N. Voskresensky, T. Tanigawa, S. Chiba and Tomoyuki Maruyama, nucl-th/0402202.

[49] T. Maruyama, T. Tatsumi, D. N. Voskresensky, T. Tanigawa and S. Chiba, Phys. Rev. **C72**, 015802 (2005).

[50] T. Maruyama, T. Tanigawa, S. Chiba, T. Tatsumi and D. N. Voskresensky, Prog. Theor. Phys. Suppl., **156**, 145 (2004).

[51] T. Maruyama, T. Tatsumi, V. N. Voskresensky, T. Tanigawa and S. Chiba, Nucl. Phys. **A749**, 186 (2005).

[52] S. Kubis, astro-ph/0407530.

[53] S. Reddy, private communication.

[54] R. G. Parr and W. Yang, *Density-Functional Theory of Atoms and Molecules* (Oxford U Press, 1989) *Density Functional Theory*, ed. E. K. U. Gross and R. M. Dreizler, Plenum Press (1995).

[55] E. Friedman, A. Gal and C. J. Batty, Nucl. Phys. **A579**, 518 (1994);
C. J. Batty, E. Friedman and A. Gal, Phys. Rep. **287**, 385 (1997).

[56] E. Friedman, A. Gal, J. Mares and A. Cieply, Phys. Rev. **C60**, 024314 (1999).

[57] T. Waas,N. Kaiser and W. Weise, Phys. Lett. **B365**, 12 (1996); Phys. Lett. **B379**, 34 (1996).
T. Waas and W. Weise, Nucl. Phys. **A625**, 287 (1997).

[58] A. Ramos and E. Oset, Nucl. Phys. **A671**, 481 (2000).

[59] J. Schaffner-Bielich, V. Koch and M. Effenberger, Nucl. Phys. **A669**, 153 (2000).

[60] L. Tolós, A. Ramos and A. Polls, Phys. Rev. **C65**, 054907 (2002).

[61] J. A. Oller, E. Oset and A. Ramos, Prog. Part. Nucl. Phys. **45**, 157 (2000).

[62] D. N. Voskresensky and A. I. Chernoutsan, Sov. J. Nucl. Phys. **27**, 742 (1978).

[63] W. D. Myers and W. J. Swiatecki, Nucl. Phys. **A601**, 141 (1996).

[64] Y. Akaishi and T. Yamazaki, Phys. Rev. C **65**, 044005 (2002);
T. Yamazaki and Y. Akaishi, Phys. Lett. **B535**, 70 (2002).

[65] A. Dote, H. Horiuchi, Y. Akaishi and T. Yamazaki, Phys. Lett. **B590**, 51 (2004); Phys. Rev. **C70**, 044313 (2004).

[66] T. Kishimoto, Phys. Rev. Lett. **83** (1999), 4701;
M. Iwasaki et al., Nucl. Instrum. Methods Phys. Res. **A473** (2001), 286.

[67] M. Iwasaki et al., Nucl. Phys. **A**, (2004) to be published;
T. Kishimoto, *ibid*;
T. Suzuki et al., Phys. Lett. **B597**, 263 (2004); nucl-ex/0310018;
Agnello et al., Phys. Rev. Lett. **94**, 212303 (2005).

[68] T. Maruyama et al., in progress.

[69] Note that we consider a linearized KN Lagrangian for simplicity, which is not chiral-symmetric.

[70] Note that only the combination $V_{\rm Coul} - \mu_e - V_0$ matters due to the gauge invariance.